Wide-band optical switch via white light cavity

Jingping Xu,[1,2,3] M. Al-Amri,[1,4] Yaping Yang,[3] Shi-Yao Zhu,[4] and M. Suhail Zubairy[2,4]

[1]*The National Center for Mathematics and Physics, KACST, P.O. Box 6086, Riyadh 11442, Saudi Arabia*

[2]*Institute of Quantum Science and Engineering (IQSE) and Department of Physics and Astronomy, Texas A&M University, College Station, Texas 77843-4242, USA*

[3]*Key Laboratory of Advanced Micro-Structure Materials, Ministry of Education, Department of Physics, Tongji University, Shanghai 200092, China*

[4]*Beijing Computational Science Research Center, Beijing 100084, China*

(Received 5 March 2012; published 21 September 2012)

We propose a device whose reflectivity can be controlled optically over a wide frequency band. To this objective, we propose a Fabry-Pérot cavity filled with a three-level atomic gas such that the effective susceptibility can be adjusted through incoherent pump and coherent driving fields. Adopting the concepts of electromagnetic-induced transparency and the white light cavity, we can control the susceptibility to break or satisfy the resonance condition over a wide frequency range, resulting in a wide-band optical switch. In addition to numerical calculation, we first give the analytical parameters, such as pump rate, and the Rabi frequency of the driven field, required for white light cavity in this paper. Using such a cavity as a wall of another cavity, we can, optically, realize a wide-band Q-switched cavity. Such a device can also be used as a new type of optical switch for quantum information.

DOI: 10.1103/PhysRevA.86.033828 PACS number(s): 42.50.Gy, 42.50.Ct, 42.15.Eq, 42.79.Ta

I. INTRODUCTION

Optical switches are an important element in many optical systems, which have the function to transform from transparent into opaque to incident light, and vice versa. In addition to their use as a usual switch, they have been applied to produce the Q-switching laser, which is used to squeeze the output pulse to achieve high peak power and narrower width. Based on the mechanical (rotating mirror), electro-optic, and acousto-optic switches, there are corresponding rotating mirror Q-switching [1], electro-optic Q-switching [2], and acousto-optic Q-switching [3] lasers. In addition to the application of optical switching on lasers, optical switches also have promising applications in quantum information. For example, two qubits trapped in two separated cavities connected by an optical fiber can generate entanglement [4]. Now if one uses an optical switch to turn f the fiber on and off, one can control the entanglement of the two qubits. Typically the mechanical, electric, and acoustic modes introduce unstable factors in the process. Therefore a pure optical switch is considered more interesting and stable.

There are several methods to adjust and control the reflectivity by external fields. Wang *et al.* added a driving field to a two-level atomic gas inside a cavity to realize an optical switch in a narrow frequency band [5]. Zhang *et al.* controlled the reflection of a probe field in Λ-type three-level atoms of cesium vapor by two counterpropagating coupling fields [6,7] and reached the maximum reflectivity of 0.6 [7]. Barak *et al.* considered an atom near a microtoroidal resonator which coupled to a fiber to control the transmission of photons through fiber [8]. Recently, an interesting phenomenon called the electromagnetic induced grating (EIG) has attracted both theoretical and experimental attention [9–11]. The idea of EIG is just to change the medium from being transparent to opaque by simply using an optical method. However, most of above-mentioned methods work at a very narrow frequency band.

In this paper, we propose a mirror consisting of a Fabry-Pérot cavity filled with three-level driven atomic gas, and define such a mirror as a cavity-made mirror. It is shown that, by adding pumping and driving fields on the atomic gas, we can control the reflectivity of such a mirror, resorting to the concepts of the electromagnetic induced transparency (EIT) [12] and the white light cavity [13–16]. This way, the total transmission properties of the mirror can be changed to near total reflection, and vice versa, in a wide frequency band. This is an interesting approach to coherently control the reflectivity of a cavity-made mirror adopting an optical method.

This paper is organized as follows: In Sec. II, we introduce the model. In Sec. III, we discuss the susceptibility of the atomic gas with pump and driving fields. In Sec. IV, we study the white light cavity condition in our model. How to realize the reflectivity-controllable mirror is discussed in Sec. V. The conclusions are presented in Sec. VI.

II. MODEL OF CAVITY-MADE MIRROR

It is well known that the susceptibility of an atomic gas can be controlled optically, such as in EIT [12] and enhanced refractive index without absorption [17]. However, using atomic gas as a uniform slab, the reflectivity at interface is small and is less sensitive to the susceptibility due to low impedance [6,7]. Here we consider a mirror consisting of an atomic gas that is confined within two metallic mirrors. A similar model of a cavity filled with two-level atomic gas was used to control the Goos-Hänchen shift [5], in which authors mainly focused on a certain frequency and considered the variation of reflectivity with the incident angle.

The scheme of the cavity-made mirror is shown in Fig. 1(a). The region between the two mirrors contains atomic gas. The level structure of the atoms inside the cavity is shown in Fig. 1(b). The reflectivity of the end mirrors is set to be $R_{\rm mirr} = 0.999$. The response of the atomic gas to an incident probe (signal) field is characterized by the susceptibility χ. The equivalent relative refractive index of atomic gas is

$$n = \sqrt{1+\chi} \tag{1}$$

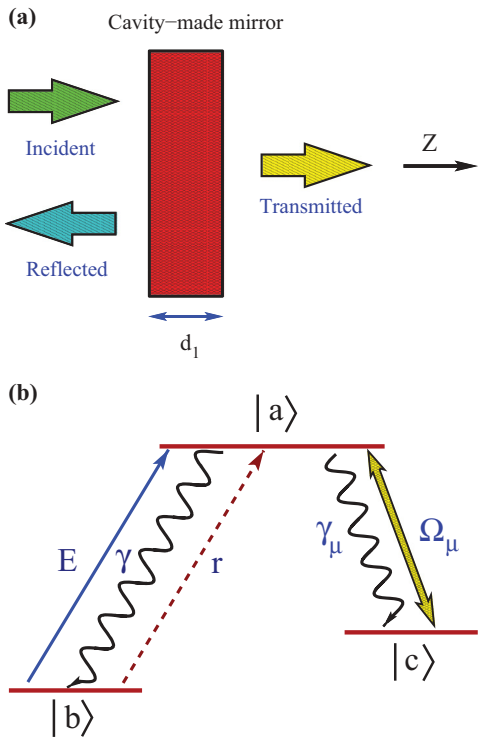

FIG. 1. (Color online) The scheme of cavity-made mirror (a) consisting of three-level atoms of the type shown in (b) filling a cavity.

and the resonance condition of the cavity is

$$\mathrm{Re}\,(n)d_1\frac{\omega_m}{c}=m\pi \quad (m=1,2,\ldots). \tag{2}$$

When the frequency ω of the incident field E is equal to the resonant frequency ω_m, the incident field can transmit through the cavity-made mirror. Otherwise, the field is reflected. Thus, for a certain frequency, we can adjust the equivalent refractive index to satisfy the resonance condition, making the cavity-made mirror transparent. However, it is hard to realize transparency for such a cavity-made mirror over a wide frequency band with usual dielectrics. Therefore, the key question here is how to control the susceptibility of the atomic gas in order for the cavity field, being resonant over a wide band, resulting in a wide-band unit transparency. In the next section, we discuss the susceptibility of the atomic gas with level structure shown in Fig. 1(b) and show that, for a certain range of parameters, it is possible to obtain an external control of reflectivity over a wide range of frequencies.

III. SUSCEPTIBILITY OF THE ATOMIC GAS

We consider a three-level atomic system in Λ configuration with one upper state $|a\rangle$ and two ground states $|b\rangle$ and $|c\rangle$ as shown in Fig. 1(b). An example of such a system is ^{133}Cs for which $|a\rangle \equiv (6\,^2P_{1/2}, F=4)$, $|b\rangle \equiv (6\,^2S_{1/2}, F=3)$, and $|c\rangle \equiv (6\,^2S_{1/2}, F=4)$. We want to calculate the response of a probing (signal) field E that is nearly resonant with the $|a\rangle \rightarrow |b\rangle$ transition by calculating the susceptibility. The level $|a\rangle$ is also coupled to the level $|c\rangle$ via a strong driving field of Rabi frequency Ω_μ. In addition, we include a pump mechanism from level $|b\rangle$ to level $|a\rangle$ with a pumping rate r. The decay rates from level $|a\rangle$ to level $|b\rangle$ and from level $|a\rangle$ to level $|c\rangle$ are assumed to be γ and γ_μ, respectively. The decay from level $|b\rangle$ to level $|c\rangle$ is ignored.

The system Hamiltonian of the three-level atoms interacting with the signal and driving fields (but ignoring the decay and pump mechanisms) is

$$\mathcal{H}=\hbar\omega_{ab}|a\rangle\langle a|+\hbar\omega_{cb}|c\rangle\langle c|-(\hbar\Omega_\mu e^{-i\omega_\mu t}|a\rangle\langle c| +\wp E e^{-i\omega t}|a\rangle\langle b|+\text{c.c.}). \tag{3}$$

Here $\wp$ is the dipole matrix element of the transition $|a\rangle \leftrightarrow |b\rangle$. In Eq. (3), we omit the off-resonant coupling of a driven field to the transition $|a\rangle \leftrightarrow |b\rangle$ and the coupling of a probe field to the transition $|a\rangle \leftrightarrow |c\rangle$. The reason is that these off-resonant interactions only introduce fast oscillation terms and have nearly no contribution to the internal state evolution after time average. After setting the following transformations: $\rho_{ab}=\tilde{\rho}_{ab}e^{i\omega t}$, $\rho_{ac}=\tilde{\rho}_{ac}e^{i\omega_\mu t}$, $\rho_{cb}=\tilde{\rho}_{cb}e^{i(\omega+\omega_\mu)t}$, $\Delta=\omega_{ab}-\omega$, and $\Delta_\mu=\omega_{ac}-\omega_\mu$ and adding the contribution of the atomic decays and the pumping rate, we get the following equations for the elements of density matrix (for derivation, see Appendix A):

$$\dot{\rho}_{aa}=-(\gamma+\gamma_\mu)\rho_{aa}+r\rho_{bb} +i\left(\frac{\wp}{\hbar}E\tilde{\rho}_{ba}+\Omega_\mu\tilde{\rho}_{ca}-\frac{\wp}{\hbar}E^*\tilde{\rho}_{ab}-\Omega_\mu^*\tilde{\rho}_{ac}\right), \tag{4a}$$

$$\dot{\rho}_{bb}=-r\rho_{bb}+\gamma\rho_{aa}-i\left(\frac{\wp}{\hbar}E\tilde{\rho}_{ba}-\frac{\wp}{\hbar}E^*\tilde{\rho}_{ab}\right), \tag{4b}$$

$$\dot{\rho}_{cc}=\gamma_\mu\rho_{aa}-i(\Omega_\mu\tilde{\rho}_{ca}-\Omega_\mu^*\tilde{\rho}_{ac}), \tag{4c}$$

$$\dot{\tilde{\rho}}_{ab}=-\gamma_{ab}\tilde{\rho}_{ab}-i\Delta\tilde{\rho}_{ab}-i\frac{\wp}{\hbar}E(\rho_{aa}-\rho_{bb})+i\Omega_\mu\tilde{\rho}_{cb}, \tag{4d}$$

$$\dot{\tilde{\rho}}_{cb}=-\gamma_{cb}\tilde{\rho}_{cb}-i(\Delta-\Delta_\mu)\tilde{\rho}_{cb}+i\Omega_\mu^*\tilde{\rho}_{ab}-i\frac{\wp}{\hbar}E\tilde{\rho}_{ca}, \tag{4e}$$

$$\dot{\tilde{\rho}}_{ca}=-\gamma_{ca}\tilde{\rho}_{ca}+i\Delta_\mu\tilde{\rho}_{ca}-i\Omega_\mu^*(\rho_{cc}-\rho_{aa})-i\frac{\wp}{\hbar}E^*\tilde{\rho}_{cb}. \tag{4f}$$

Here $\gamma_{ca}=\gamma_{ab}=(\gamma+\gamma_\mu)/2$ and $\gamma_{cb}=0$. We solve this set of equations for $\tilde{\rho}_{ab}$ in the steady state to the first order of the probe field E, which is labeled as $\tilde{\rho}_{ab}^{(1)}$. Thus the resulting expression for $\tilde{\rho}_{ab}^{(1)}$ is

$$\tilde{\rho}_{ab}^{(1)}=\frac{\wp E}{\hbar}\frac{[(\Delta-\Delta_\mu)]\left(\rho_{aa}^{(0)}-\rho_{bb}^{(0)}\right)+\Omega_\mu\tilde{\rho}_{ca}^{(0)}}{[|\Omega_\mu|^2-\Delta(\Delta-\Delta_\mu)]+i[(\Delta-\Delta_\mu)\gamma_{ab}]}, \tag{5}$$

where $\tilde{\rho}_{\alpha\beta}^{(0)}$ is the zeroth order of the matrix element in the probe field E. The corresponding expression for the susceptibility [18] is given by

$$\chi=\mathcal{A}\frac{[(\Delta-\Delta_\mu)]\left(\rho_{aa}^{(0)}-\rho_{bb}^{(0)}\right)+\Omega_\mu\tilde{\rho}_{ca}^{(0)}}{[|\Omega_\mu|^2-\Delta(\Delta-\Delta_\mu)]+i[(\Delta-\Delta_\mu)\gamma_{ab}]}, \tag{6}$$

where $\mathcal{A}=N\wp^2/\epsilon_0\hbar$, and N is number density of atom gas. The steady-state values of $\rho_{aa}^{(0)}$, $\rho_{bb}^{(0)}$, and $\tilde{\rho}_{ca}^{(0)}$ are obtained using the rest of the equations in Eqs. (4) by omitting the elements multiplied by E and incorporating the normalization condition.

We then obtain (for derivation, see Appendix B)

$$\rho_{cc}^{(0)} = \frac{r\left[\gamma_\mu\left(\gamma_{ca}^2+\Delta_\mu^2\right)+2\gamma_{ca}|\Omega_\mu|^2\right]}{2(2r+\gamma)\gamma_{ca}|\Omega_\mu|^2+r\gamma_\mu\left(\gamma_{ca}^2+\Delta_\mu^2\right)}, \tag{7a}$$

$$\rho_{bb}^{(0)} = \frac{2\gamma\gamma_{ca}|\Omega_\mu|^2}{2(2r+\gamma)\gamma_{ca}|\Omega_\mu|^2+r\gamma_\mu\left(\gamma_{ca}^2+\Delta_\mu^2\right)}, \tag{7b}$$

$$\rho_{aa}^{(0)} = \frac{2r\gamma_{ca}|\Omega_\mu|^2}{2(2r+\gamma)\gamma_{ca}|\Omega_\mu|^2+r\gamma_\mu\left(\gamma_{ca}^2+\Delta_\mu^2\right)}, \tag{7c}$$

$$\tilde{\rho}_{ca}^{(0)} = \frac{-i\Omega_\mu^*\left(\rho_{cc}^{(0)}-\rho_{aa}^{(0)}\right)}{\gamma_{ca}-i\Delta_\mu}. \tag{7d}$$

It is clear that if the pumping rate r is larger than the decay rate of the transition $|a\rangle \to |b\rangle$, i.e., $r > \gamma$, the population inversion happens, i.e., $\rho_{aa}^{(0)} > \rho_{bb}^{(0)}$. Moreover, at resonance, i.e., $\Delta_\mu = \Delta = 0$, $\chi = \mathcal{A}\frac{\Omega_\mu \tilde{\rho}_{ca}^{(0)}}{|\Omega_\mu|^2}$ and coherence $\tilde{\rho}_{ca}^{(0)}$ is purely imaginary and contributes to the absorption or gain. A lower absorption or even net gain can be obtained at resonance when $\tilde{\rho}_{ca}^{(0)} = 0$ or $\rho_{aa}^{(0)} = \rho_{cc}^{(0)}$. This can happen when we turn off the pumping or increase the Rabi frequency of the driving field. Though the above results are obtained under certain approximations, they are reliable under the condition when the probe field is much weaker than the driving field. A comparison of the results based on the above approximation with the exact numerical calculation of the evolution of matrix element according to Eqs. (4) is shown in Appendix C. Our approximate results are in full agreement with the exact numerical results when the probe field is weak.

The emphasis here is that by adjusting the pumping rate r and the driving field Ω_μ, we can control the population inversion and the coherence $\tilde{\rho}_{ca}^{(0)}$. Consequently, we find a neat way to control the susceptibility χ. We adopt $\gamma_\mu = 0.2\gamma$, $\gamma_{ca} = \gamma_{ab} = (\gamma_\mu + \gamma)/2 = 1.1\gamma$, and $\Delta_\mu = 0$ as the operating parameters in this paper. For lower density of the atomic gas, we set $\mathcal{A} = \gamma$ here. Next we determine the susceptibility as a function of the frequency of the incident field under different pump rates and the driving fields.

A. Absence of pump, $r = 0$

In this case, the steady values in Eqs. (7) have values $\rho_{bb}^{(0)} = 1$ and the rest are zero. In other words, the atom is in the ground state $|b\rangle$ all the time. The susceptibility becomes

$$\chi = \frac{-\gamma\Delta}{(|\Omega_\mu|^2-\Delta^2)+i\Delta\gamma_{ab}}. \tag{8}$$

The susceptibility as a function of the frequency of the driving field is plotted in Fig. 2. This is just the phenomena of EIT. At the resonant frequency $\omega = \omega_{ab}$, susceptibility is exactly zero. The slope at $\omega = \omega_{ab}$ is positive and its value decreases with increasing the driving field Ω_μ.

B. Pump with $r < \gamma$

In this case, $\tilde{\rho}_{aa}^{(0)} - \tilde{\rho}_{bb}^{(0)} < 0$. The coherence $\tilde{\rho}_{ca}^{(0)}$ approaches zero with increasing Ω_μ. The susceptibility is plotted in

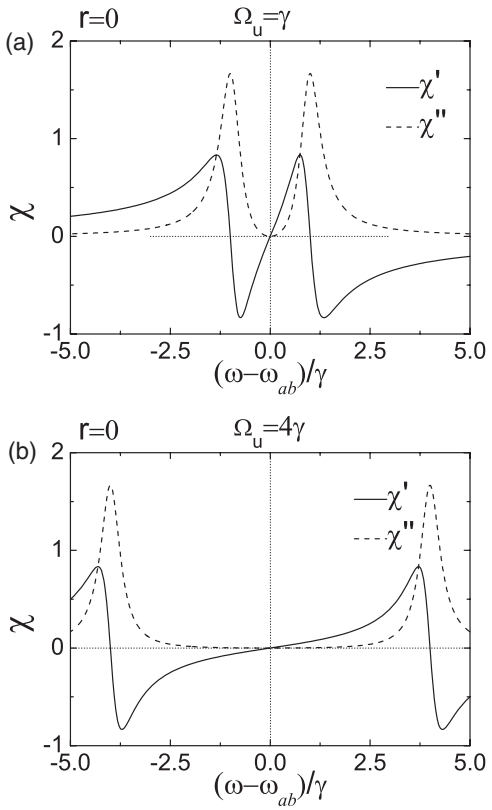

FIG. 2. The susceptibility as a function of the frequency of the signal field in the absence of the pump field $r = 0$ with (a) $\Omega_\mu = \gamma$ and (b) $\Omega_\mu = 4\gamma$. Solid (dashed) line refers to the real (imaginary) part of the susceptibility.

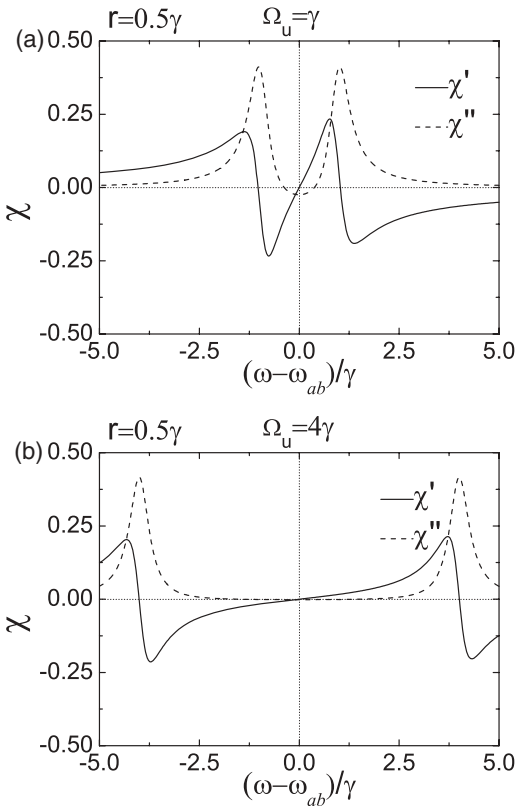

FIG. 3. The susceptibility as a function of the frequency of the signal field with pumping rate $r = 0.5\gamma$ with (a) $\Omega_\mu = \gamma$ and (b) $\Omega_\mu = 4\gamma$. Solid (dashed) line refers to the real (imaginary) part of the susceptibility.

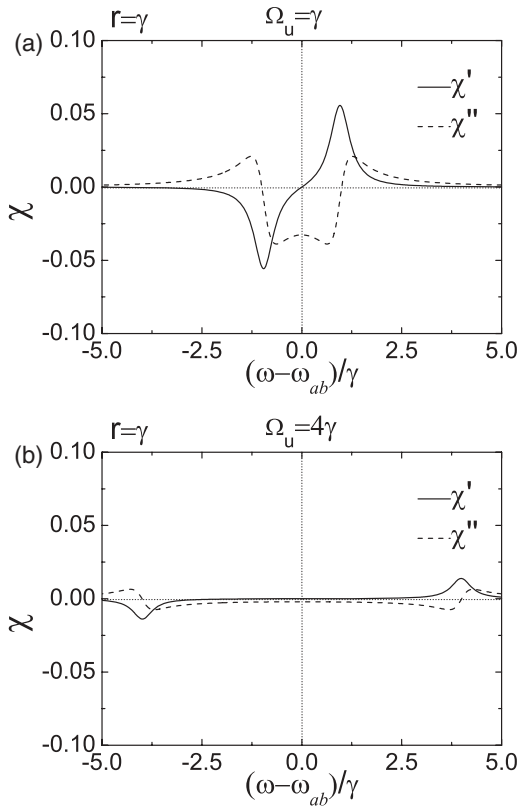

FIG. 4. The susceptibility as a function of the frequency of the detected field with pump $r = \gamma$ with (a) $\Omega_\mu = \gamma$ and (b) $\Omega_\mu = 4\gamma$. Solid (dashed) line refers to the real (imaginary) part of the susceptibility.

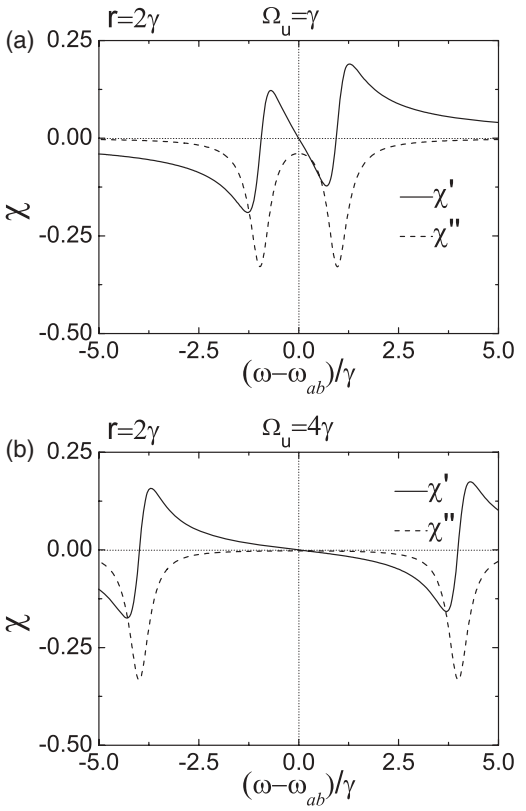

FIG. 5. The susceptibility as a function of the frequency of the signal field for pumping rate $r = 2\gamma$ with (a) $\Omega_\mu = \gamma$ and (b) $\Omega_\mu = 4\gamma$.

Fig. 3 and both real and imaginary parts are similar to the EIT case.

The amplitude of the susceptibility decreases as r approaches γ. Due to the influence of $\tilde{\rho}_{ca}^{(0)}$, the imaginary part of susceptibility is negative at $\omega = \omega_{ab}$ whose amplitude decreases with Ω_μ.

C. Pump with $r = \gamma$

In this case, $\tilde{\rho}_{aa}^{(0)} - \tilde{\rho}_{bb}^{(0)} = 0$, and the susceptibility becomes

$$\chi = \frac{\gamma \Omega_\mu \tilde{\rho}_{ca}^{(0)}}{(|\Omega_\mu|^2 - \Delta^2) + i\Delta\gamma_{ab}}, \tag{9}$$

which is very different from the EIT case. We plot the real and imaginary parts of the susceptibility in Fig. 4 and see that, for $\Omega_\mu = 4\gamma$, the susceptibility is essentially zero for the entire range of signal frequencies.

D. Pump with $r > \gamma$

When the pumping rate is larger than the decay rate, i.e., $r > \gamma$, the population inversion takes place and we obtain $\tilde{\rho}_{aa}^{(0)} - \tilde{\rho}_{bb}^{(0)} > 0$. If we omit $\tilde{\rho}_{ca}^{(0)}$ in the expression (6) of the susceptibility, the resulting expression is similar to Eq. (8) except multiplying by the factor -1. Thus we obtain negative dispersion. According to Eq. (6) the real part of the susceptibility is proportional to the population inversion while its imaginary part is proportional to $\tilde{\rho}_{ca}^{(0)}$.

It is clear from Eqs. (7) that the population inversion $\tilde{\rho}_{aa}^{(0)} - \tilde{\rho}_{bb}^{(0)}$ relates to the ratio of r to γ, while $\tilde{\rho}_{ca}^{(0)}$ relates to the ratio of Ω_μ to γ_μ. We plot the susceptibility as a function of frequency of the probe field for different pumping rates r and different Rabi frequencies of the driving field Ω_μ in Figs. 5 and 6.

From above, it is clear that it is easy to control the slope of the susceptibility through Ω_μ, while the gain can be decreased by increasing the Rabi frequency of the driving field. This is seen by comparing the dashed curves in Fig. 6(a) with 6(b). We list the population inversion $\tilde{\rho}_{aa}^{(0)} - \tilde{\rho}_{bb}^{(0)}$ and $\tilde{\rho}_{ca}^{(0)}$ for different cases in Table I. In the next section, we discuss how to control the susceptibility to realize the resonance or off resonance of a cavity-made mirror over a wide range of frequencies.

IV. WHITE LIGHT CAVITY CONDITION

In a Fabry-Pérot cavity, only certain discrete frequencies can be exactly resonant. If the cavity is filled with a medium that possesses a negative dispersion and cancels the frequency dependence of the phase delay, a continuous range of frequencies can be resonant at the same time. Such a cavity is called a white light cavity [13]. There were several papers concerning the white light cavity using the bifrequency Raman gain [14–16]. However, in this paper, we adopt another method to realize the white light cavity, the reason being that our model can easily be transformed into an EIT model just by turning off the pump.

From Eq. (2), ω_m are discrete frequencies for the usual dielectric. If we want to get a resonance frequency band, the refractive index of the medium should satisfy

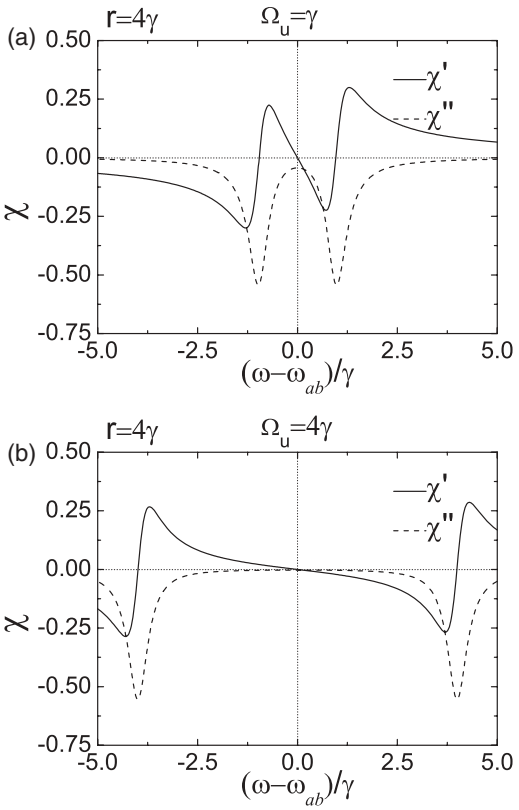

FIG. 6. The susceptibility as a function of the frequency of the signal field for pumping rate $r = 4\gamma$ with (a) $\Omega_\mu = \gamma$ and (b) $\Omega_\mu = 4\gamma$.

the equation $\partial\{\mathrm{Re}\,[n(\omega)]\,\omega\}/\partial\omega = 0$ or $\partial \mathrm{Re}\,[n(\omega)]/\partial\omega = -\mathrm{Re}\,[n(\omega)]/\omega$. Here we focus on the frequency region near ω_{ab}. From the results in Figs. 5 and 6, we see that the susceptibility χ near ω_{ab} can be neglected for both real and imaginary parts, and then the white light cavity condition is [13,16]

$$\partial\,\mathrm{Re}\,[n(\omega)]/\partial\omega|_{\omega=\omega_{ab}} = -1/\omega_{ab}. \tag{10}$$

The key is to determine the required Rabi frequency of the driving field $\Omega_{\mu W}$ satisfying Eq. (10). To obtain the required $\Omega_{\mu W}$ satisfying the white light cavity condition, we approximate $\partial\,\mathrm{Re}\,[n(\omega)]/\partial\omega|_{\omega=\omega_{ab}}$ by $\mathrm{Re}\,[n(\omega_{ab}+\gamma) - n(\omega_{ab}-\gamma)]/2\gamma$. In addition, as χ near ω_{ab} is much smaller, it is reasonable to use the Taylor expansion $n(\omega) \approx 1 + \chi'/2 + i\chi''/2$. The resulting equation for $\Omega_{\mu W}$ is

$$\chi'(\omega_{ab}+\gamma) - \chi'(\omega_{ab}-\gamma) = -4\gamma/\omega_{ab}. \tag{11}$$

TABLE I. Population inversion and $\rho_{ca}^{(0)}$ for different values of r and Ω_μ.

		$\rho_{aa}^{(0)} - \rho_{bb}^{(0)}$	$\rho_{ca}^{(0)}$
$r = 2\gamma$	$\Omega_\mu = \gamma$	0.196	$-0.04i$
	$\Omega_\mu = 2\gamma$	0.188	$-0.02i$
	$\Omega_\mu = 4\gamma$	0.199	$-0.01i$
$r = 4\gamma$	$\Omega_\mu = \gamma$	0.325	$-0.04i$
	$\Omega_\mu = 2\gamma$	0.331	$-0.02i$
	$\Omega_\mu = 4\gamma$	0.333	$-0.01i$

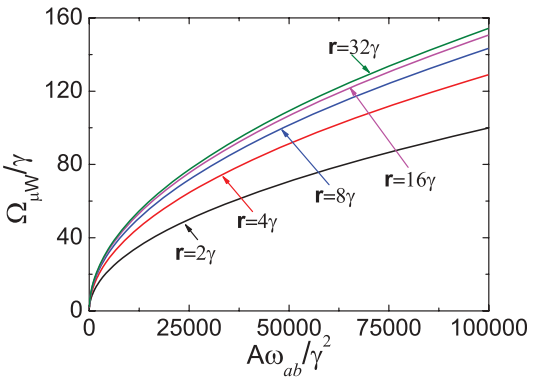

FIG. 7. (Color online) The required $\Omega_{\mu W}$ for the white light condition as a function of $A\omega_{ab}$ for different pumping rate r. $\gamma_\mu = 0.2\gamma$, $\gamma_{ac} = \gamma_{ab} = (\gamma + \gamma_\mu)/2 = 1.1\gamma$, and $\gamma_{cb} = 0$.

Here χ' is the real part of susceptibility. On inserting the expression of χ into Eq. (11) and performing some simplifications (shown in Appendix D), we get the required $\Omega_{\mu W}$ satisfying white light condition. The resulting expression is

$$\Omega_{\mu W} = \sqrt{-\frac{b}{3a} + \frac{1}{3a}\sqrt[3]{\frac{1}{2}(\alpha+\sqrt{\beta})} + \frac{1}{3a}\sqrt[3]{\frac{1}{2}(\alpha-\sqrt{\beta})}}, \tag{12a}$$

$$\alpha = 9abc - 2b^3 - 27a^2d, \tag{12b}$$

$$\beta = \alpha^2 + 4(3ac - b^2)^3, \tag{12c}$$

$$a = 4(2r+\gamma)\gamma_{ca}, \tag{12d}$$

$$b = 2\gamma_{ca}[r\gamma\gamma_{ca} - A\omega_0(r-\gamma) - 4\gamma^2(2r+\gamma)] \tag{12e}$$

$$c = \gamma_{ca}\big[2A\omega_0(r-\gamma)\gamma^2 + A\omega_0\gamma_{ab}r\gamma_\mu - 4\gamma^2 r\gamma_{ca}\gamma_\mu + 4(2r+\gamma)\big(\gamma^2+\gamma_{ab}^2\big)\gamma^2\big], \tag{12f}$$

$$d = 2r\gamma_\mu\gamma_{ca}^2\gamma^2\big(\gamma^2+\gamma_{ab}^2\big). \tag{12g}$$

This is an exact solution for the white light cavity condition. With the known atomic level structure and the pumping rate, we can calculate the required $\Omega_{\mu W}$ satisfying the white light cavity condition. This avoids the tedious process judged from reflectivity by using different values of Ω_μ [13].

With the parameters $\gamma_\mu = 0.2\gamma$ and $\gamma_{ca} = \gamma_{ab} = 1.1\gamma$, we plot $\Omega_{\mu W}$ as a function of $A\omega_{ab}$ (with $A = N\wp^2/\epsilon_0\hbar$) for different values of the pumping rate r in Fig. 7. It is clear that $\Omega_{\mu W}$ increases with $A\omega_{ab}$ and pump rate r. However, there seems to be a limitation on $\Omega_{\mu W}$ for increasing the pumping rate. It is noticed that the difference between the case of $r = 16$ and the case of $r = 32$ is negligible. This can be understood by the fact that r can only affect the population inversion which has a maximum value 1.

For usual atomic gas, $A = \gamma$ and $\omega_{ab} \propto 10^6\gamma$. Therefore $\Omega_{\mu W}$ is about $10^2\gamma$. It is clear from Figs. 5 and 6 that the band-width of the white light condition (linear dependence of χ to ω) has the same order as $\Omega_{\mu W}$. Therefore in our model, the linewidth of the white light cavity is about $10^2\gamma$.

V. REFLECTIVITY OF THE CAVITY-MADE MIRROR

In this section, we show how the above results obtained for a white light cavity can be used to realize a controllable reflectivity of the cavity-made mirror for a wide range of

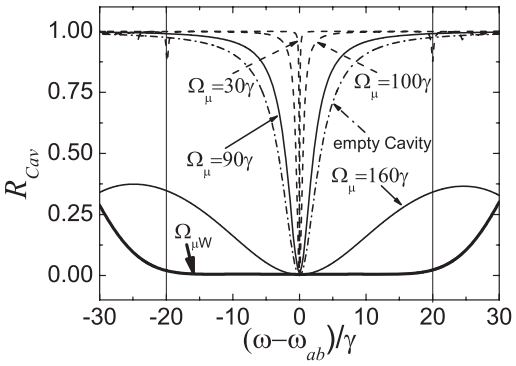

FIG. 8. The reflectivity of the cavity-made mirror as a function of the frequency of the signal field for different driving fields and pumping rates. The dashed lines refer to the absence of pump $r = 0$. The solid lines refer to nonzero pumping with $r = 32\gamma$. The thickest line corresponds to the white light condition with $\Omega_{\mu W} = 154.88\gamma$. Empty refers to empty cavity without atomic gas. The length of the cavity is $d_1 = 100c\pi/\omega_{ab}$.

frequencies. The reflectivity of the cavity-made mirror shown in Fig. 1(a) is given by

$$R_{\rm cav} = \left| r_{\rm mirr} + \frac{T_{\rm mirr} r_{\rm mirr} e^{2i(d\omega_{ab}/c)[1-(\Delta/\omega_{ab})]n(\Delta)}}{1 - R_{\rm mirr} e^{2i(d\omega_{ab}/c)[1-(\Delta/\omega_{ab})]n(\Delta)}} \right|^2. \quad (13)$$

As mentioned above $R_{\rm mirr} = 0.999$, $T_{\rm mirr} = -0.001$, and $r_{\rm mirr} = \sqrt{R_{\rm mirr}}$. We set $d = 100c\pi/\omega_{ab}$, i.e., the length of the cavity is 50 wavelengths at ω_{ab}. Other parameters are the same as before.

We first present the case of EIT which corresponds to the absence of the pumping rate with $r = 0$. This is shown as the dashed lines in Fig. 8. It is clear that the EIT effect can sharpen the linewidth of the spectrum. For $r = 0$ and $\Omega_\mu = 30\gamma$ the reflectivity is high in the frequency band except for a narrow frequency range close to ω_{ab}. The linewidth in such a case is much narrower than the linewidth of the empty cavity, which is about 6.4γ. This means that, in the presence of the driving field, the linewidth decreases as compared to the case of the empty cavity. This is easy to understand from Fig. 2 where we see that an addition of the driving field can induce a positive slope for the real part of the susceptibility. Such a slope enhances the off-resonant nature of the field detuning from ω_{ab}. However, the stronger the driving field, the milder the slope. Therefore the linewidth for a strong driving field tends to approach that for an empty cavity.

Next we consider the case when we add the pump. From Figs. 5 and 6, we see that the pump leads to a negative slope of susceptibility which can compensate for the resonance condition (2). According to the solid lines in Fig. 8, we see that when the driving field satisfies the white light cavity, $\Omega_{\mu W} = 154.88\gamma$, there is a wide band with a width of about 40γ in which the reflectivity is near 0. When Ω_μ is different from $\Omega_{\mu W}$, the reflectivity is nonvanishing for all frequencies except near $\omega = \omega_{ab}$. Therefore we realize optical switch with a bandwidth of about 40γ, i.e., by adding a pumping field and adjusting the driving field at $\Omega_{\mu W}$. Here the reflectivity of the cavity-made mirror approaches zero in the frequency band $|\omega - \omega_{ab}| = 20\gamma$. Also if we cancel the pump and decrease the Rabi frequency of the driven field to $\Omega_\mu = 30\gamma$, the reflectivity of the cavity-made mirror can be almost unity for the same band except around $\omega = \omega_{ab}$. Adopting the data in Ref. [6] that $\gamma \approx 2\pi \times 4.6$ MHZ, the effective band of our optical switch can reach 1 GHZ.

Note that for such a case, there are small dips in reflectivity near $|\omega - \omega_{ab}| = 20\gamma$. The reason for these dips is that the absorption induced phase satisfied the resonance condition in Eq. (2), while the absorption prevents the transmission. This results in having a dip.

From Fig. 8, we see that the linewidth in the spectrum of reflectivity in the absence of a pump is always smaller than that for the empty cavity. However, for the case of a nonzero pumping rate, the situation is more complex. The slopes of the phases for the empty cavity and cavity containing atomic gas, respectively, are

$$\frac{d\phi_0}{d\omega} = \frac{d_1}{c}, \quad (14)$$

$$\left.\frac{d\phi_A}{d\omega}\right|_{\omega=\omega_0} = \frac{d_1}{c}\left(n + \omega\partial n/\partial\omega|_{\omega=\omega_0}\right) \approx \frac{d_1}{c}\left(1 + \omega\partial n/\partial\omega|_{\omega=\omega_0}\right). \quad (15)$$

Therefore, if $|d\phi_A/d\omega|_{\omega=\omega_0}| < d\phi_0/d\omega$, the linewidth of the spectrum for cavity containing atomic gas is larger than that for the empty cavity. Otherwise, the linewidth is smaller than the empty cavity. For the case of absence of the pump, $\partial n/\partial\omega > 0$ so that the linewidth is always narrower than that for the empty cavity. However, with the increase of Ω_μ, and $\partial n/\partial\omega \to 0$, the linewidth tends to that for an empty cavity.

For the case of pump, $\partial n/\partial\omega < 0$. Therefore, when $|\omega\partial n/\partial\omega|_{\omega=\omega_0}| < 2$, the linewidth is larger than the empty cavity; such cavity is a white light cavity in general. Otherwise, the linewidth is narrower than that for the empty cavity and has the same result as when the pump is absent. When $\omega\partial n/\partial\omega|_{\omega=\omega_0} = -2$, this case has the same linewidth as that of the empty cavity. Similar to Eqs. (12) the required Rabi frequency of an empty cavity $\Omega_{\mu E}$ has the same expression as Eqs. (12) except for the different coefficients.

In Fig. 9(a), we plot the required Rabi frequency $\Omega_{\mu E}$ for an empty cavity as a function of $A\omega_{ab}$ in the presence of the pump. For certain $A\omega_{ab}$ and the pump rate r, the linewidth of $\Omega_\mu < \Omega_{\mu E}$ is narrower than that of the empty cavity, whereas the linewidth of $\Omega_\mu > \Omega_{\mu E}$ is larger than that of the empty cavity. We illustrate this behavior in Fig. 9(b), where we compare the reflectivity of a cavity-made mirror for different Ω_μ. For the required $\Omega_{\mu E} \approx 92\gamma$, it is clear that the corresponding linewidth is nearly the same as that of the empty cavity. For $\Omega_\mu = 80\gamma$, the corresponding linewidth gets narrower than that of an empty cavity, while it is larger when $\Omega_\mu = 100\gamma$. Therefore, with the pump and the driving field, we can adjust the linewidth of the cavity containing atom gas.

Moreover, for the empty cavity shown in Fig. 10(a) while ignoring the absorption inside the cavity, the Q factor of the cavity can be expressed by the reflectivity of the two walls as Refs. [19,20]

$$Q(w) = \frac{\pi}{-\ln\sqrt{R_L(\omega)R_R}}. \quad (16)$$

Here $R_L(\omega) = R_{\rm cav}$ is the reflectivity of the left cavity-made mirror, and $R_R = R_{\rm mirr} = 0.999$. The Q factor as a function

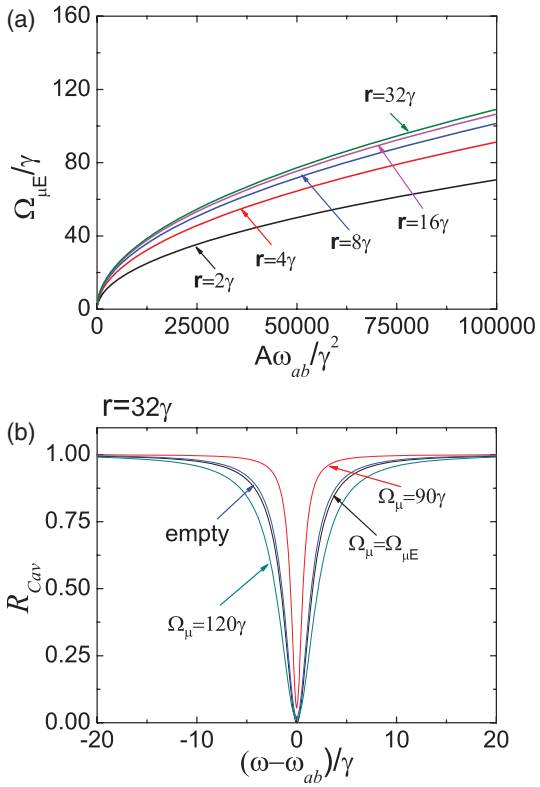

FIG. 9. (Color online) (a) The required $\Omega_{\mu E}$ for an empty cavity as a function of $A\omega_{ab}$ for different pumping rate r. (b) The reflectivity of a cavity-made mirror as a function of the detected field for different Ω_μ with $r = 32\gamma$, $A\omega_{ab} = 10^6\gamma^2$, and $\Omega_{\mu E} = 92\gamma$.

of the detected field for different driving and pump fields are shown in Fig. 10(b).

From Fig. 10(b), it is clear that the Q factor can be controlled easily through the driving and the pump fields applied to the cavity-made mirror. Curve (C) refers to the Q factor of the cavity-made mirror of the two same mirrors with $R_{\text{mirr}} = 0.999$, and its value is $Q = 3140$. When we apply a pump and set the driving field as $\Omega_\mu = \Omega_{\mu W}$, the Q factor moves close to 1 in the band $|\omega - \omega_{ab}| < 20\gamma$. When we turn off the pump and set the driving field as $\Omega_\mu = 30\gamma$, the Q factor gets larger than 313 except in the bands $|\omega - \omega_{ab}| < 0.56\gamma$ and $|\omega - \omega_{ab}| > 19.4\gamma$. Therefore, our cavity-made mirror acts as a wide-band optical switch.

VI. CONCLUSION

We proposed a wide-band optical switch which is made of a cavity that contains a three-level atomic gas. By adjusting the pumping rate and the driving field, the susceptibility can be controlled at the resonant or the off-resonant signal field over a wide-band frequency. We show that controlling the pumping rate can lead to a positive dispersion in the EIT regime and negative dispersion in the white light cavity limit. We obtain the exact white light cavity condition which determines the required driving field for a given set of other parameters. When turning off the pumping field and adding the driving field, such a cavity-made mirror has high reflectivity but for a narrow band near the resonant frequency. However, by turning on the

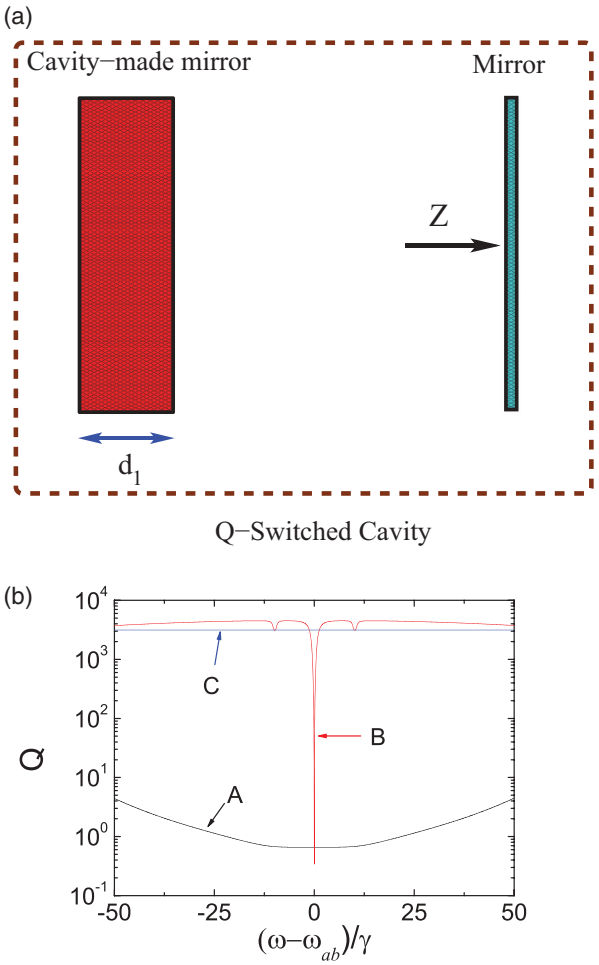

FIG. 10. (Color online) The scheme of a Q-switched cavity. (b) Q factor as a function of the frequency of the detected field. A refers to the case of $r = 32\gamma$ and $\Omega_\mu = \Omega_{\mu W}$, while B refers to the case of $r = 0$ and $\Omega_\mu = 30\gamma$. C refers to the case when the cavity is made of two same mirrors $R_{\text{mirr}} = 0.999$. The parameters of the cavity-made mirror are the same as above.

pumping field and adding the required driving field for a white light cavity, the cavity mirror can become transparent to a very wide band of frequencies. This way we show that this laser cavity mirror can be used as an optical switch, where we can control its Q factor for a broadband of frequency adopting entirely an all-optical method.

ACKNOWLEDGMENTS

This work is supported by a grant from the King Abdulaziz City for Science and Technology (KACST), the National Science Foundation of China (Grants No. 91021012, No. 10904113, No. 11174026, and No. 11274242), and CNKBRSF (No. 2011CB922203). M.A. would like to thank Qingqing Sun for simulating discussions, and gratefully acknowledges the hospitality at CSRC where part of this work was done. The research of M.S.Z. is supported by NPRP Grant No. 4-346-1-061 from the Qatar National Research Fund (QNRF).

APPENDIX A: THE DERIVATION OF EQS. (4)

The Hamiltonian $\mathcal{H}$ in Eq. (3) can be expressed in the matrix notation as

$$\mathcal{H} = \begin{pmatrix} \hbar\omega_{ab} & -\wp E e^{-i\omega t} & -\hbar\Omega_\mu e^{-i\omega_\mu t} \\ -\wp E^* e^{i\omega t} & 0 & 0 \\ -\hbar\Omega_\mu^* e^{i\omega_\mu t} & 0 & \hbar\omega_{cb} \end{pmatrix}. \tag{A1}$$

It then follows that

$$\mathcal{H}\rho = \begin{pmatrix} \hbar\omega_{ab} & -\wp E e^{-i\omega t} & -\hbar\Omega_\mu e^{-i\omega_\mu t} \\ -\wp E^* e^{i\omega t} & 0 & 0 \\ -\hbar\Omega_\mu^* e^{i\omega_\mu t} & 0 & \hbar\omega_{cb} \end{pmatrix} \begin{pmatrix} \rho_{aa} & \rho_{ab} & \rho_{ac} \\ \rho_{ba} & \rho_{bb} & \rho_{bc} \\ \rho_{ca} & \rho_{cb} & \rho_{cc} \end{pmatrix} \tag{A2}$$

$$= \begin{pmatrix} \hbar\omega_{ab}\rho_{aa} - \wp E e^{-i\omega t}\rho_{ba} & \hbar\omega_{ab}\rho_{ab} - \wp E e^{-i\omega t}\rho_{bb} & \hbar\omega_{ab}\rho_{ac} - \wp E e^{-i\omega t}\rho_{bc} \\ -\hbar\omega_\mu e^{-i\omega_\mu t}\rho_{ca} & -\hbar\omega_\mu e^{-i\omega_\mu t}\rho_{cb} & -\hbar\omega_\mu e^{-i\omega_\mu t}\rho_{cc} \\ -\wp E^* e^{i\omega t}\rho_{aa} & -\wp E^* e^{i\omega t}\rho_{ab} & -\wp E^* e^{i\omega t}\rho_{ac} \\ -\hbar\Omega_\mu^* e^{i\omega_\mu t}\rho_{aa} + \hbar\omega_{cb}\rho_{ca} & -\hbar\Omega_\mu^* e^{i\omega_\mu t}\rho_{ab} + \hbar\omega_{cb}\rho_{cb} & -\hbar\Omega_\mu^* e^{i\omega_\mu t}\rho_{ac} + \hbar\omega_{cb}\rho_{cc} \end{pmatrix}, \tag{A3}$$

$$\rho\mathcal{H} = \begin{pmatrix} \rho_{aa} & \rho_{ab} & \rho_{ac} \\ \rho_{ba} & \rho_{bb} & \rho_{bc} \\ \rho_{ca} & \rho_{cb} & \rho_{cc} \end{pmatrix} \begin{pmatrix} \hbar\omega_{ab} & -\wp E e^{-i\omega t} & -\hbar\Omega_\mu e^{-i\omega_\mu t} \\ -\wp E^* e^{i\omega t} & 0 & 0 \\ -\hbar\Omega_\mu^* e^{i\omega_\mu t} & 0 & \hbar\omega_{cb} \end{pmatrix} \tag{A4}$$

$$= \begin{pmatrix} \hbar\omega_{ab}\rho_{aa} - \wp E^* e^{i\omega t}\rho_{ab} - \hbar\omega_\mu^* e^{i\omega_\mu t}\rho_{ac} & -\wp E e^{-i\omega t}\rho_{aa} & -\hbar\Omega_\mu e^{-i\omega_\mu t}\rho_{aa} + \hbar\omega_{cb}\rho_{ac} \\ \hbar\omega_{ab}\rho_{ba} - \wp E^* e^{i\omega t}\rho_{bb} - \hbar\omega_\mu^* e^{i\omega_\mu t}\rho_{bc} & -\wp E e^{-i\omega t}\rho_{ba} & -\hbar\Omega_\mu e^{-i\omega_\mu t}\rho_{ba} + \hbar\omega_{cb}\rho_{bc} \\ \hbar\omega_{ab}\rho_{ca} - \wp E^* e^{i\omega t}\rho_{cb} - \hbar\omega_\mu^* e^{i\omega_\mu t}\rho_{cc} & -\wp E e^{-i\omega t}\rho_{ca} & -\hbar\Omega_\mu e^{-i\omega_\mu t}\rho_{ca} + \hbar\omega_{cb}\rho_{cc} \end{pmatrix}. \tag{A5}$$

We obtain the following equations of motion for the elements of the density matrix from the Schrodinger equation $\dot{\rho} = -\frac{i}{\hbar}[\mathcal{H}, \rho]$:

$$\dot{\rho}_{aa} = i\left(\frac{\wp}{\hbar} E e^{-i\omega t}\rho_{ba} + \Omega_\mu e^{-i\omega_\mu t}\rho_{ca} - \frac{\wp}{\hbar} E^* e^{i\omega t}\rho_{ab} - \Omega_\mu^* e^{i\omega_\mu t}\rho_{ac}\right), \tag{A6a}$$

$$\dot{\rho}_{bb} = -i\left(\frac{\wp}{\hbar} E e^{-i\omega t}\rho_{ba} - \frac{\wp}{\hbar} E^* e^{i\omega t}\rho_{ab}\right), \tag{A6b}$$

$$\dot{\rho}_{cc} = -i\left(\Omega_\mu e^{-i\omega_\mu t}\rho_{ca} - \Omega_\mu^* e^{i\omega_\mu t}\rho_{ac}\right), \tag{A6c}$$

$$\dot{\rho_{ab}} = -i\omega_{ab}\rho_{ab} - i\frac{\wp}{\hbar} E e^{-i\omega t}(\rho_{aa} - \rho_{bb}) + i\Omega_\mu e^{-i\omega_\mu t}\rho_{cb}, \tag{A6d}$$

$$\dot{\rho}_{cb} = -i\omega_{cb}\rho_{cb} + i\Omega_\mu^* e^{i\omega_\mu t}\rho_{ab} - i\frac{\wp}{\hbar} E e^{-i\omega t}\rho_{ca}, \tag{A6e}$$

$$\dot{\rho}_{ca} = -i\omega_{ca}\rho_{ca} - i\Omega_\mu^* e^{i\omega_\mu t}(\rho_{cc} - \rho_{aa}) - i\frac{\wp}{\hbar} E^* e^{i\omega t}\rho_{cb}. \tag{A6f}$$

Next we set $\rho_{ab} = \tilde{\rho}_{ab} e^{-i\omega t}$, $\rho_{ac} = \tilde{\rho}_{ac} e^{-i\omega_\mu t}$, $\rho_{cb} = \tilde{\rho}_{cb} e^{-i(\omega_\mu + \omega)t}$, $\Delta = \omega_{ab} - \omega$, and $\Delta_\mu = \omega_{ac} - \omega_\mu$. After including the decay and the pumping rates, we obtain

$$\dot{\rho}_{aa} = -(\gamma + \gamma_\mu)\rho_{aa} + r\rho_{bb} + i\left(\frac{\wp}{\hbar} E\tilde{\rho}_{ba} + \Omega_\mu\tilde{\rho}_{ca} - \frac{\wp}{\hbar} E^*\tilde{\rho}_{ab} - \Omega_\mu^*\tilde{\rho}_{ac}\right), \tag{A7a}$$

$$\dot{\rho}_{bb} = -r\rho_{bb} + \gamma\rho_{aa} - i\left(\frac{\wp}{\hbar} E\tilde{\rho}_{ba} - \frac{\wp}{\hbar} E^*\tilde{\rho}_{ab}\right), \tag{A7b}$$

$$\dot{\rho}_{cc} = \gamma\rho_{aa} - i(\Omega_\mu\tilde{\rho}_{ca} - \Omega_\mu^*\tilde{\rho}_{ac}), \tag{A7c}$$

$$\dot{\tilde{\rho}}_{ab} = -\gamma_{ab}\tilde{\rho_{ab}} - i\Delta\tilde{\rho_{ab}} - i\frac{\wp}{\hbar} E(\rho_{aa} - \rho_{bb}) + i\Omega_\mu\tilde{\rho}_{cb}, \tag{A7d}$$

$$\dot{\tilde{\rho}}_{cb} = -\gamma_{cb}\tilde{\rho}_{cb} - i(\Delta - \Delta_\mu)\tilde{\rho}_{cb} + \Omega_\mu^*\tilde{\rho}_{ab} - i\frac{\wp}{\hbar} E\tilde{\rho}_{ca}, \tag{A7e}$$

$$\dot{\tilde{\rho}}_{ca} = -\gamma_{ca}\tilde{\rho}_{ca} + i\Delta_\mu\tilde{\rho}_{ca} - i\Omega_\mu^*(\rho_{cc} - \rho_{aa}) - i\frac{\wp}{\hbar} E^*\tilde{\rho}_{cb}. \tag{A7f}$$

APPENDIX B: THE DERIVATION OF SUSCEPTIBILITY EQS. (6)

In this Appendix we calculate $\tilde{\rho}_{ab}$ in the steady state to first order in the probe field E. Such approximation result of $\tilde{\rho}_{ab}$ is marked by $\tilde{\rho}_{ab}^{(1)}$. We focus on Eqs. (4d) and (4e), in which all the elements multiplied by E are redefined as $\rho_{\alpha\beta}^{(0)}$. The resulting equations are

$$0 = -(i\Delta + \gamma_{ab})\tilde{\rho}_{ab}^{(1)} - i\frac{\wp}{\hbar}E\left(\rho_{aa}^{(0)} - \rho_{bb}^{(0)}\right) + i\Omega_\mu\tilde{\rho}_{cb}^{(1)}, \tag{B1a}$$

$$0 = -[i(\Delta - \Delta_\mu) + \gamma_{cb}]\tilde{\rho}_{cb}^{(1)} + \Omega_\mu^*\tilde{\rho}_{ab}^{(1)} - i\frac{\wp}{\hbar}E\tilde{\rho}_{ca}^{(0)}, \tag{B1b}$$

with the solution

$$\tilde{\rho}_{ab}^{(1)} = \frac{\wp}{\hbar}E\frac{[(\Delta - \Delta_\mu) - i\gamma_{cb}]\left(\rho_{aa}^{(0)} - \rho_{bb}^{(0)}\right) + \Omega_\mu\rho_{ca}^{(0)}}{[|\Omega_\mu|^2 - \Delta(\Delta - \Delta_\mu) + \gamma_{ab}\gamma_{cb}] + i(\Delta\gamma_{cb} + (\Delta - \Delta_\mu)\gamma_{ab})}. \tag{B2}$$

Then, according to the definition of susceptibility, we obtain

$$\chi = \frac{N\wp\tilde{\rho}_{ab}^{(1)}}{\epsilon_0 E} = \frac{N\wp^2}{\epsilon_0\hbar}\frac{[(\Delta - \Delta_\mu) - i\gamma_{cb}]\left(\rho_{aa}^{(0)} - \rho_{bb}^{(0)}\right) + \Omega_\mu\rho_{ca}^{(0)}}{[|\Omega_\mu|^2 - \Delta(\Delta - \Delta_\mu) + \gamma_{ab}\gamma_{cb}] + i(\Delta\gamma_{cb} + (\Delta - \Delta_\mu)\gamma_{ab})}. \tag{B3}$$

Finally, we should get the value of $\rho_{aa}^{(0)}$, $\rho_{bb}^{(0)}$, and $\rho_{ca}^{(0)}$. They are actually the zeroth order of the matrix elements in the probe field E, and satisfy the equations as

$$-(\gamma + \gamma_\mu)\rho_{aa}^{(0)} + r\rho_{bb}^{(0)} + i\left(\Omega_\mu\tilde{\rho}_{ca}^{(0)} - \Omega_\mu^*\tilde{\rho}_{ac}^{(0)}\right) = 0, \tag{B4a}$$

$$-r\rho_{bb}^{(0)} + \gamma\rho_{aa}^{(0)} = 0, \tag{B4b}$$

$$\gamma_\mu\rho_{aa}^{(0)} - i\left(\Omega_\mu\tilde{\rho}_{ca}^{(0)} - \Omega_\mu^*\tilde{\rho}_{ac}^{(0)}\right) = 0, \tag{B4c}$$

$$-(\gamma_{ca} - i\Delta_\mu)\tilde{\rho}_{ca}^{(0)} - i\Omega_\mu^*\left(\rho_{cc}^{(0)} - \rho_{aa}^{(0)}\right) = 0, \tag{B4d}$$

$$\rho_{aa}^{(0)} + \rho_{bb}^{(0)} + \rho_{cc}^{(0)} = 1. \tag{B4e}$$

The above equations come from Eqs. (4a)–(4c) and (4f) with omitting the elements multiplied by E, and the normalization condition. The solutions are

$$\rho_{cc}^{(0)} = \frac{r\left[\gamma_\mu\left(\gamma_{ca}^2 + \Delta_\mu^2\right) + 2\gamma_{ca}|\Omega_\mu|^2\right]}{2(2r + \gamma)\gamma_{ca}|\Omega_\mu|^2 + r\gamma_\mu\left(\gamma_{ca}^2 + \Delta_\mu^2\right)]}, \tag{B5a}$$

$$\rho_{bb}^{(0)} = \frac{2\gamma\gamma_{ca}|\Omega_\mu|^2]}{2(2r + \gamma)\gamma_{ca}|\Omega_\mu|^2 + r\gamma_\mu\left(\gamma_{ca}^2 + \Delta_\mu^2\right)]}, \tag{B5b}$$

$$\rho_{aa}^{(0)} = \frac{2r\gamma_{ca}|\Omega_\mu|^2]}{2(2r + \gamma)\gamma_{ca}|\Omega_\mu|^2 + r\gamma_\mu\left(\gamma_{ca}^2 + \Delta_\mu^2\right)]}, \tag{B5c}$$

$$\tilde{\rho}_{ca}^{(0)} = \frac{-i\Omega_\mu^*\left(\rho_{cc}^{(0)} - \rho_{aa}^{(0)}\right)}{\gamma_{ca} - i\Delta_\mu}. \tag{B5d}$$

APPENDIX C: THE NUMERICAL RESULT OF EQS. (4)

In this Appendix, we present exact numerical solutions of Eqs. (4), and then compare the results with the approximate results of Eqs. (5)–(7). The motivation here is to show that our results are consistent and reliable.

The key to our approximation is that the probe field is much weaker than the driving field. We therefore set $\frac{\wp}{\hbar}E = 0.001\Omega_\mu$ in this Appendix. Other common parameters are $\gamma_\mu = 0.2\gamma$, $\gamma_{ca} = \gamma_{ab} = 1.1\gamma$, $\Omega_\mu = \gamma$, $\Delta_\mu = 0$, and $\Delta = 0$. We will compare the evolution of the matrix elements $\tilde{\rho}_{ab}$, $\rho_{aa} - \rho_{bb}$, and ρ_{ca} with the corresponding approximate results shown in Eqs. (5) and (7). Since $\tilde{\rho}_{ab}$ is linearly proportional to the probe field, we adopt a scaled quantity $\tilde{\rho}_{ab}/B$ with $B = \frac{\wp E}{\hbar\gamma}$ to replace $\tilde{\rho}_{ab}$. In the steady state, $\tilde{\rho}_{ab}/B$ is just the susceptibility χ.

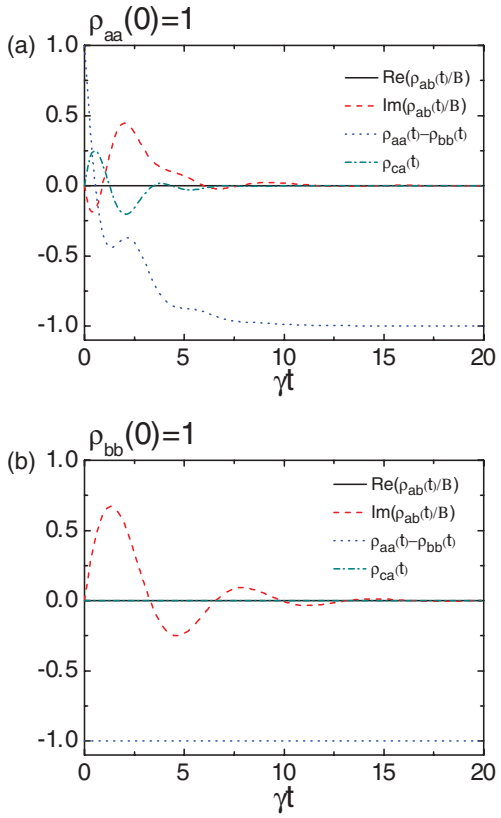

FIG. 11. (Color online) The evolution of the matrix elements based on exact numerical solution of Eqs. (4) when $r = 0$. The atom is initially prepared in levels (a) $|a\rangle$ and (b) $|b\rangle$.

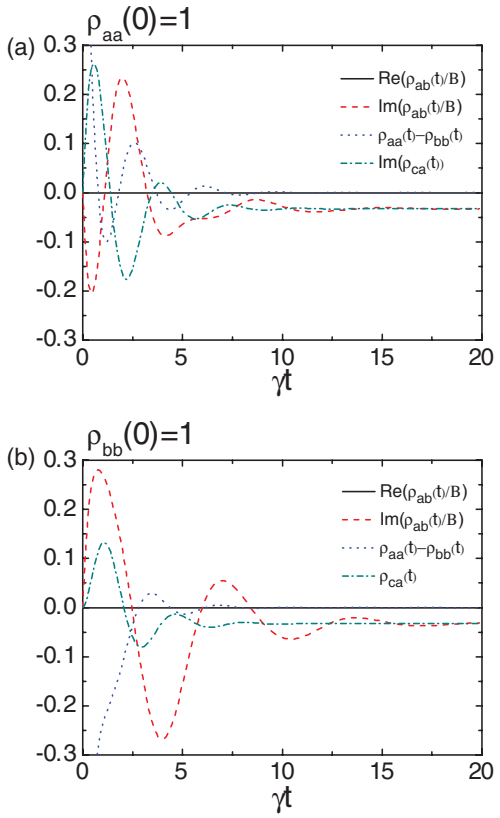

FIG. 12. (Color online) The evolution of the matrix elements based on exact numerical solutions of Eqs. (4) when $r = \gamma$. The atom is initially prepared in levels (a) $|a\rangle$ and (b) $|b\rangle$.

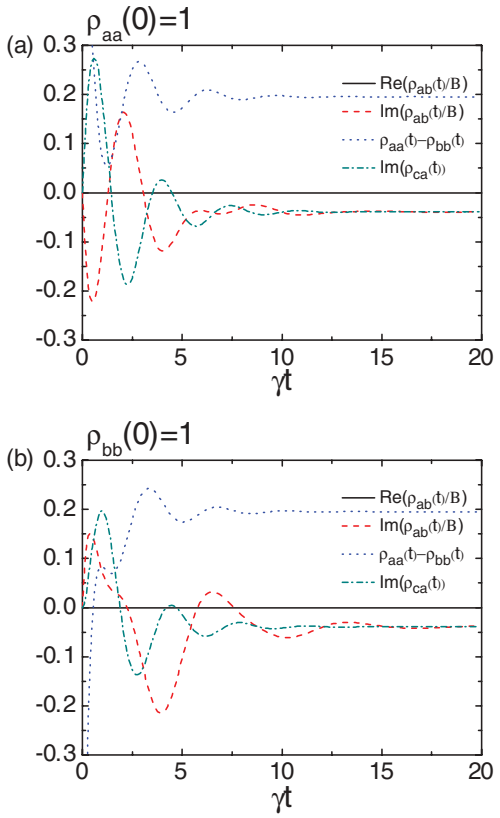

FIG. 13. (Color online) The evolution of the matrix elements based on exact numerical solutions of Eqs. (4) when $r = 2\gamma$. The atom is initially prepared in levels (a) $|a\rangle$ and (b) $|b\rangle$.

For comparison, we show the results of three different cases as follows:

First case: The absence of the pump with $r = 0$. The relative approximate results are $\rho_{aa}^{(0)} - \rho_{bb}^{(0)} = -1$, $\rho_{ca}^{(0)} = 0$, and $\tilde{\rho}_{ab}^{(1)} = 0$. The numerical evolution of the corresponding matrix elements in Eqs. (4) are shown in Fig. 11 under two different initial states. It is shown that the evolution of the matrix elements is initially different for different initial states. However, they tend to have the same value as the time increases [see Figs. 11(a) and 11(b) for comparison]. More importantly, the steady-state values of the matrix elements are consistent with that of the approximate values as predicted above.

Second case: The pump rate is the same as the decay rate, i.e., $r = \gamma$. The approximate results are $\rho_{aa}^{(0)} - \rho_{bb}^{(0)} = 0$, $\rho_{ca}^{(0)} = -i0.033$, and $\tilde{\rho}_{ab}^{(1)}/B = -i0.033$. The exact evolution of the corresponding matrix elements is shown in Fig. 12 under two different initial states. It is shown that the matrix element tends to the approximated result as predicted above.

Third case: The pump rate is two times the decay rate, i.e., $r = 2\gamma$. The approximate results are $\rho_{aa}^{(0)} - \rho_{bb}^{(0)} = 0.196$, $\rho_{ca}^{(0)} = -i0.039$, and $\tilde{\rho}_{ab}^{(1)}/B = -i0.039$. In Fig. 13, we show the exact numerical results of the evolution of the matrix elements under two different initial states. As before, the steady values of the matrix elements are consistent with our approximate results.

In view of the three cases discussed above, we have demonstrated that our approximate results in Eqs. (5)–(7) are consistent with the exact numerical results and that our approximation is reliable when the probe field is weak. The main condition here is that $\frac{\wp}{\hbar}E < 0.01\Omega_\mu$. However, only when $\frac{\wp}{\hbar}E > 0.1\Omega_\mu$, do our approximate results deviate appreciably from the exact numerical results.

APPENDIX D: THE DERIVATION OF THE RABI FREQUENCY $\Omega_{\mu W}$ FOR THE WHITE LIGHT CAVITY

In order to get the resonance for any frequency, we need $\partial\{\mathrm{Re}\,[n(\omega)]\,\omega\}/\partial\omega = 0$, which is $\partial\,\mathrm{Re}\,[n(\omega)]/\partial\omega = -\mathrm{Re}\,[n(\omega)]/\omega$. Here we focus on the frequency region near ω_{ab}. As the frequency is close to ω_{ab}, both the real and the imaginary parts of the susceptibility can be neglected. Hence, the white light cavity condition is

$$\partial\,\mathrm{Re}\,[n(\omega)]/\partial\omega|_{\omega=\omega_{ab}} = -1/\omega_{ab}. \tag{D1}$$

To get the required $\omega_{\mu W}$ for a white light cavity, we transform $\partial\,\mathrm{Re}\,[n(\omega)]/\partial\omega|_{\omega=\omega_{ab}}$ into $\mathrm{Re}\,[n(\omega_{ab}+\gamma) - n(\omega_{ab}-\gamma)]/2\gamma$. In addition, as χ moves close to ω_{ab}, its value gets smaller. It is reasonable to use the Taylor expansion $n(\omega) = 1 + \chi'/2 + i\chi''/2$. We then obtain the equation for $\Omega_{\mu W}$,

$$\chi'(\omega_{ab}+\gamma) - \chi'(\omega_{ab}-\gamma) = -4\gamma/\omega_{ab}. \tag{D2}$$

With the resonance case of the driving field $\Delta_\mu = 0$, the equivalent susceptibility becomes

$$\chi = \frac{N\wp^2}{\epsilon_0\hbar}\frac{\Delta\left(\rho_{aa}^{(0)} - \rho_{bb}^{(0)}\right) + \Omega_\mu\tilde{\rho}_{ca}^{(0)}}{(|\Omega_\mu|^2 - \Delta^2) + i\Delta\gamma_{ab}}. \tag{D3}$$

Its imaginary part is

$$\chi' = \frac{N\wp^2}{\epsilon_0\hbar}\frac{\Delta\left(\rho_{aa}^{(0)} - \rho_{bb}^{(0)}\right)(|\Omega_\mu|^2 - \Delta^2) - i\Delta\gamma_{ab}\Omega_\mu\tilde{\rho}_{ca}^{(0)}}{(|\Omega_\mu|^2 - \Delta^2)^2 + \Delta^2\gamma_{ab}^2} \tag{D4}$$

with

$$\rho_{aa}^{(0)} - \rho_{bb}^{(0)} = \frac{2(r-\gamma)\gamma_{ca}|\Omega_\mu^*|^2}{2(2r+\gamma)\gamma_{ca}|\Omega_\mu^*|^2 + r\gamma_\mu\gamma_{ca}^2}, \tag{D5a}$$

$$\tilde{\rho}_{ca}^{(0)} = \frac{-i\Omega_\mu^* r\gamma_\mu\gamma_{ca}}{2(2r+\gamma)\gamma_{ca}|\Omega_\mu^*|^2 + r\gamma_\mu\gamma_{ca}^2}. \tag{D5b}$$

It follows that, on inserting Eqs. (D5) and (D4) into Eqs. (D3) and (D2), we obtain the cubic equation for $|\Omega_\mu|^2$:

$$a|\Omega_\mu|^6 + b|\Omega_\mu|^4 + c|\Omega_\mu|^2 + d = 0, \tag{D6}$$

where we set $A = N\wp^2/\epsilon_0\hbar$, $a = 4(2r+\gamma)\gamma_{ca}$, $b = 2\gamma_{ca}[r\gamma\gamma_{ca} - A\omega_0(r-\gamma) - 4\gamma^2(2r+\gamma)]$, $c = \gamma_{ca}[2A\omega_0(r-\gamma)\gamma^2 + A\omega_0\gamma_{ab}r\gamma_\mu - 4\gamma^2 r\gamma_{ca}\gamma_\mu + 4(2r+\gamma)(\gamma^2+\gamma_{ab}^2)\gamma^2]$, and $d = 2r\gamma_\mu\gamma_{ca}^2\gamma^2(\gamma^2+\gamma_{ab}^2)$. Its real root is

$$\Omega_{\mu W} = \sqrt{-\frac{b}{3a} + \frac{1}{3a}\sqrt[3]{\frac{1}{2}(\alpha+\sqrt{\beta})} + \frac{1}{3a}\sqrt[3]{\frac{1}{2}(\alpha-\sqrt{\beta})}}, \tag{D7a}$$

$$\alpha = 9abc - 2b^3 - 27a^2d, \tag{D7b}$$

$$\beta = \alpha^2 + 4(3ac - b^2)^3. \tag{D7c}$$

[1] M. Skorczakowski *et al.*, Laser Phys. Lett. **7**, 498 (2010).
[2] W. K. Chang, Y. H. Chen, and J. W. Chang, Opt. Lett. **35**, 2687 (2010).
[3] T. Shigeki, M. Masanao, and S. Seiji, Opt. Lett. **36**, 2812 (2011).
[4] P. Peng and F.-L. Li, Phys. Rev. A **75**, 062320 (2007).
[5] L.-G. Wang, M. Ikram, and M. S. Zubairy, Phys. Rev. A **77**, 023811 (2008).
[6] J.-X. Zhang, H.-T. Zhou, D.-W. Wang, and S.-Y. Zhu, Phys. Rev. A **83**, 053841 (2011).
[7] H.-T. Zhou, D.-W. Wang, D. Wang, J.-X. Zhang, and S.-Y. Zhu, Phys. Rev. A **84**, 053835 (2011).
[8] B. Dayan, A. S. Parkins, T. Aoki, E. P. Ostby, K. J. Vahala, and H. J. Kimble, Science **319**, 1062 (2008).
[9] A. W. Brown and M. Xiao, Opt. Lett. **30**, 699 (2005).
[10] D. Katrin, M. L. Spani, R. Rolf-Hermann, and D. Karsten, Opt. Lett. **33**, 983 (2008).
[11] B. In-Ho, M. Han Seb, K. Min-Koeung, L. Lim, and K. J. Bog, Opt. Express **18**, 1389 (2010).
[12] K.-J. Boller, A. Imamoglu, and S. E. Harris, Phys. Rev. Lett. **66**, 2593 (1991).
[13] R.-H. Rinkleff and A. Wicht, Phys. Scr., **T118**, 85 (2005).
[14] G. S. Pati, M. Salit, K. Salit, and M. S. Shahriar, Phys. Rev. Lett. **99**, 133601 (2007).
[15] J. Zhang, X. Wei, G. Hernandez, and Y. Zhu, Phys. Rev. A. **81**, 033804 (2010).
[16] Qingqing Sun, M. S. Shahriar, and M. S. Zubairy, Phys. Rev. A **81**, 033826 (2010).
[17] M. O. Scully, Phys. Rev. Lett. **67**, 1855 (1991).
[18] M. Fleischhauer, C. H. Keitel, M. O. Scully, Chang Su, B. T. Ulrich, and Shi-Yao Zhu, Phys. Rev. A **46**, 1468 (1992).
[19] A. Yariv, *Quantum Electronics*, 3rd ed. (Wiley, New York, 1988), pp. 147–148.
[20] M. O. Scully and M. S. Zubairy, *Quantum Optics* (Cambridge University Press, Cambrige, England, 1997).